International Journal of Power Electronics and Drive System (IJPEDS)
Vol. 7, No. 1, March 2016, pp. 28~44
ISSN: 2088-8694

Constant Frequency Torque Controller for DTC with Multilevel Inverter of Induction Machines

Norjulia Mohamad Nordin[1], Naziha Ahmad Azli[2], Nik Rumzi Nik Idris[3], Nur Huda Ramlan[4], Tole Sutikno[5]
[1,2,3] Universiti Teknologi Malaysia, Faculty of Electrical Engineering, Skudai, Johor Bahru, Malaysia
[4] Universiti Malaysia Pahang, Faculty of Electrical and Electronics, Pekan, Pahang, Malaysia
[5] Department of Electrical Engineering, Universitas Ahmad Dahlan, Yogyakarta, Indonesia

Article Info

Article history:

Received Oct 22, 2015
Revised Jan 7, 2016
Accepted Jan 23, 2016

Keyword:

Constant switching frequency
Direct torque control
Induction machines
Multilevel inverter
Torque Controller

ABSTRACT

Direct Torque Control using multilevel inverter (DTC-MLI) with hysteresis controller suffers from high torque and flux ripple and variable switching frequency. In this paper, a constant frequency torque controller is proposed to enhance the DTC-MLI performance. The operational concepts of the constant switching frequency torque controller of a DTC-MLI system followed by the simulation results and analysis are presented. The proposed system significantly improves the DTC drive in terms of dynamic performance, smaller torque and flux ripple, and retains a constant switching frequency.

Corresponding Author:

Norjulia Binti Mohamad Nordin,
Department of Electrical Power Engineering,
Faculty of Electrical Engineering, Universiti Teknologi Malaysia,
81310 Skudai, Johor, Malaysia.
Email: norjulia@fke.utm.my / norjulia@utm.my

1. INTRODUCTION

Since it has been introduced in early 1980s [1], Direct Torque Control (DTC) has gained its popularity in electrical drives research area. Recently, the application of high-power medium voltage in AC drives has shown rapid development. Thus, the use of multilevel inverters in DTC scheme has become an important structure for further development and improvement. Numerous technical papers have shown a superior performance of DTC scheme using multilevel inverters [2-34].

By utilizing the multilevel inverter in DTC scheme, the choices of voltage vectors that can be used to control the torque and flux are increased. As a result, more precise control can be obtained. Several control method have been proposed for DTC scheme using multilevel inverter (DTC-MLI); hysteresis-based and non-hysteresis-based such as predictive control strategy [11, 15, 17, 18, 20, 22, 26, 27, 30], space vector modulation strategy [2, 4, 8-10, 14, 21, 28, 29, 33] and fuzzy logic control strategy [3, 5, 7, 19, 31, 34-36].

The employment of hysteresis-based control strategy in discrete implementation has led to high torque ripple even with a small hysteresis band. This is due to the delay in sampling time. Besides that, it created a variable switching frequency of the switching devices which leads to an unpredictable harmonics current.

As a result, some researchers preferred to use non-hysteresis-based control strategy. Significant improvements are accomplished in terms of flux and torque ripple and devices switching frequency. However it involves a complex mathematical equations and algorithm which has led to the complexity of the DTC-MLI scheme and high computational burden particularly when the multilevel inverter's level is increased.

In [12], the DTC-MLI scheme employs a multilevel hysteresis controller. It shows some significant improvements, however the power devices switching frequency are varies and the torque and flux ripple can still be considered as high. A PI-constant switching frequency (PI-CSF) torque controller for DTC was initially introduced in [37, 38]. The PI-CSF torque controller was replacing the conventional hysteresis controller while maintaining the use of lookup-table. However it has been used for DTC with conventional 3-phase inverter.

In this work, the PI-CSF torque controller is utilized in DTC-MLI system. Figure 1 shows a proposed system block diagram. The proposed controller consists of a PI controller and a triangular carrier signal. The constant switching frequency is obtained by comparing the PI controller output with the triangular carrier signals. In this scheme, the proposed controller will replaced the multilevel hysteresis torque controller. The proposed system is employed a 5-level cascaded H-Bridge multilevel inverter (CHMI) as a power converter. The multiple isolated DC sources in CHMI are particularly suitable for an electric vehicle (EV) application since the power source for an EV can be obtained from the battery modules.

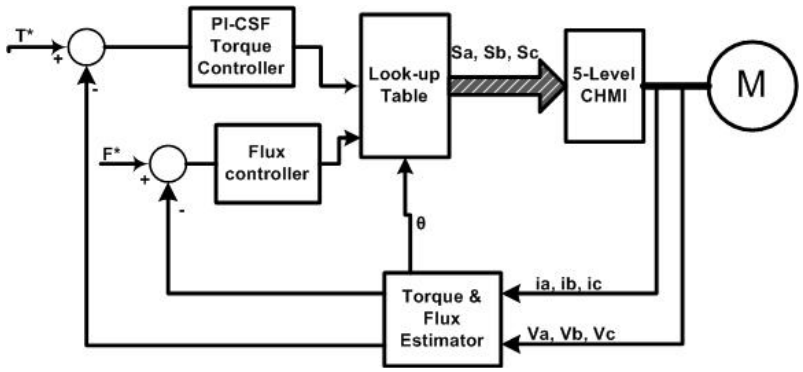

Figure 1. Proposed system block diagram

In this paper, the operational concept of PI-CSF torque controller utilized in DTC-MLI system followed by simulation results of the proposed system is presented. Furthermore the experimental results are disclosed to validate the simulation results together with the analysis on the proposed system performance. The results have shown that superior dynamic performance, smaller torque and flux ripples and constant device switching frequency are achieved.

2. MULTILEVEL INVERTER

A 5-level cascaded H-Bridge multilevel inverter (CHMI) consists of 2 cells of H-Bridge inverter connected in cascaded form with separated DC sources. Figure 2 shows a configuration of 5-level CHMI. The number of voltage level, L, for CHMI can be determined by

$$L = 2m + 1 \quad (1)$$

Where m is a number of cell per phase. Each H-bridge cell produced V_{jm} output voltage, where j denotes the phases; a, b, c. Since the cells are connected in series, the total output voltage for each phase would be

$$V_{aN} = \sum_{m=1}^{2} V_{am} \quad (2)$$

$$V_{bN} = \sum_{m=1}^{2} V_{bm} \quad (3)$$

$$V_{cN} = \sum_{m=1}^{2} V_{cm} \quad (4)$$

V_{aN}, V_{bN} and V_{cN} is the voltage output per phase with respect to the neutral, N. By considering each cell produce $\{-V_{DC}, 0, V_{DC}\}$, based on (2), (3) and (4), each phase will produce a 5-level output voltage;

$$V_{aN} = V_{bN} = V_{cN} = \{-2V_{DC}, -1\,V_{DC}, 0, 1\,V_{DC}, -2V_{DC}\} \quad (5)$$

In space phasor form, the output voltage, $\mathbf{V_S}$, that generated by the inverter can be defined as

$$V_S(t) = \frac{2}{3}\left(V_{aN}(t) + aV_{bN}(t) + a^2V_{cN}(t)\right) \quad (6)$$

Where $a = e^{j2\pi/3}$ and $a^2 = e^{j4\pi/3}$. In d-q form, the output voltage can be expressed as

$$V_{sd} = \frac{1}{3}(2V_{aN} - V_{bN} - V_{cN}) \quad (7)$$

$$V_{sq} = \frac{1}{\sqrt{3}}(V_{bN} - V_{cN}) \quad (8)$$

Considering equation (5), (6) and (7), there exist 125 combinations of phase voltage with 61 voltage vectors generated for 5-level CHMI. The higher the level of multilevel inverter, the higher the number of the voltage vector generated, thus giving more degrees of freedom in choosing voltage vectors for control purposes. Figure 3 and Figure 4 shows a voltage vector map on d-q plane generated from 5-level CHMI and the configuration of the induction machines fed by 5-level CHMI, respectively.

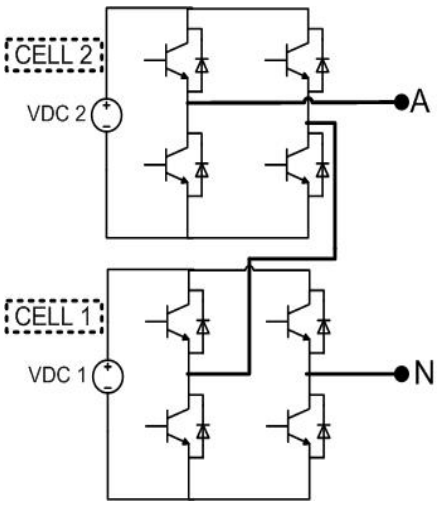

Figure 2. 5-level cascaded H-bridge multilevel inverter (CHMI)

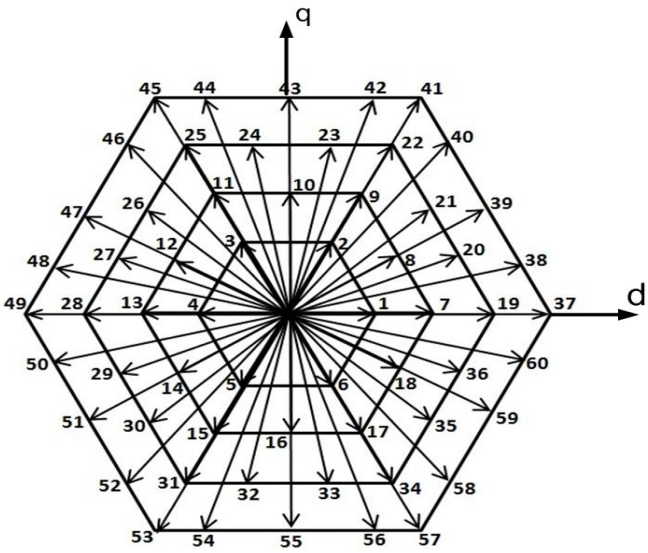

Figure 3. Voltage vector map on d-q plane

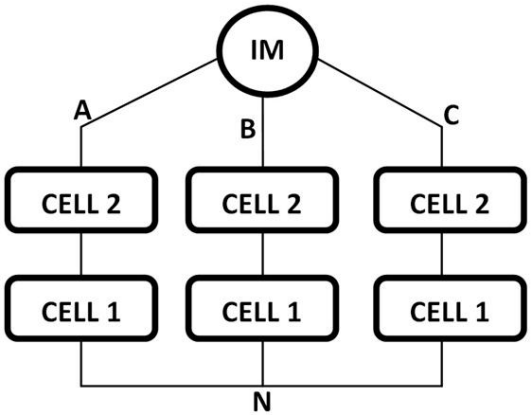

Figure 4. 3-phase induction machine fed by 5-level CHMI

3. STRUCTURE AND MODELING OF THE DTC WITH CONSTANT SWITCHING FREQUENCY

To analyze the DTC drive in terms of its switching frequency, the induction machine is modeled using the following equations. These equations are written in general reference frame.

$$\overline{v_s^g} = R_s \overline{\imath_s^g} + \frac{d\overline{\psi_s^g}}{dt} + j\omega_g \overline{\psi_s^g} \tag{9}$$

$$0 = R_r \overline{\imath_r^g} + \frac{d\overline{\psi_r^g}}{dt} + j\left(\omega_g - \omega_r\right)\overline{\psi_r^g} \tag{10}$$

$$\overline{\psi_s^g} = L_s \overline{\imath_s^g} + L_m \overline{\imath_r^g} \tag{11}$$

$$\overline{\psi_r^g} = L_r \overline{\imath_r^g} + L_m \overline{\imath_s^g} \tag{12}$$

The superscript "g" in the above equations denotes that the quantities are referred to the rotating general reference frame. In the above equations, $\overline{v_s^g}$, $\overline{\imath_s^g}$ and $\overline{\imath_r^g}$ are the stator voltage, stator current and rotor current, respectively. R_s, R_r, $\overline{\psi_s^g}$ and $\overline{\psi_r^g}$ are the stator resistances, rotor resistances, stator flux linkages and rotor flux linkages, respectively. ω_g is the general reference speed and ω_r is the rotor speed. L_s, L_r and L_m are the stator self-inductance, rotor self-inductance and mutual self-inductance respectively.
The torque and mechanical dynamics of the induction machines are modeled as follows:

$$J\,\frac{d\omega_m}{dt} = J\,\frac{2}{p}\frac{d\omega_r}{dt} = T_e - T_{load} \tag{13}$$

$$T_e = \frac{3}{2}\frac{p}{2}\overline{\psi_s^g} \times \overline{\imath_s^g} \tag{14}$$

Where T_e is the electromagnetic torque, T_{load} is the torque load, J is the moment of inertia, p is the number of pole and ω_m is the mechanical rotor speed.

By using (9) – (14) in the stationary reference frame, the positive and negative torque slope are obtained by [39, 40]

$$\frac{dT_e^+}{dt} = -T_e\left(\frac{1}{\sigma\tau_s} + \frac{1}{\sigma\tau_r}\right) + \frac{3}{2}\frac{p}{2}\frac{L_m}{\sigma L_s L_r}(\overline{V_s} - j\omega_r\overline{\psi_s}) \cdot j\psi_r \tag{15}$$

$$\frac{dT_e^-}{dt} = -T_e\left(\frac{1}{\sigma\tau_s} + \frac{1}{\sigma\tau_r}\right) - \frac{3}{2}\frac{p}{2}\frac{L_m}{\sigma L_s L_r}(j\omega_r\overline{\psi_s}) \cdot j\psi_r \tag{16}$$

Where σ is the total flux linkage factor, τ_s is the stator time constant and τ_r is the rotor time constant. In (16), it is assumes that the zero voltage vectors are selected in order to reduce the torque. The instantaneous stator flux frequency can be obtained in terms of the average synchronous frequency and duty ratio [38]. Therefore (15) and (16) can be written in the stator flux reference frame as follows:

$$\frac{dT_e^+}{dt} = -A\,T_e + B\,V_s^{\psi_s} + K\left(\frac{\omega_e}{d} - \omega_r\right) \tag{17}$$

$$\frac{dT_e^-}{dt} = -A\,T_e - K\,\omega_r \tag{18}$$

Where

$$A = \left(\frac{1}{\sigma\tau_s} + \frac{1}{\sigma\tau_r}\right) \tag{19}$$

$$B = \left(\frac{3p}{4}\right)\left(\frac{L_m}{\sigma L_s L_r}\right)\psi_s \tag{20}$$

$$K = \left(\frac{3p}{4}\right)\left(\frac{L_m}{\sigma L_s L_r}\right)\psi_s\psi_r^{\psi_s} \tag{21}$$

In (17) and (18), it is assumed that the q components of the particular voltage vector are zero and the stator and rotor fluxes are constant which means that the voltage vectors are tangential to the circular stator flux locus. Finally, the equation (17) and (18) are averaged and simplified to give

$$\frac{dT_e}{dt} = -A\,T_e + B\,V_s^{\psi_s} d + K\left(\omega_{slip}\right) \tag{22}$$

4. THE PROPOSED CONTROLLER

The proposed torque controller is employed as an alternative to the hysteresis-based controller with the benefit of operating at constant switching frequency with low torque ripple. The proposed controller consist of 6 triangular waveform generators, 6 comparators and a proportional-integral (PI) controller. Figure 5 shows the configuration of the proposed torque controller.

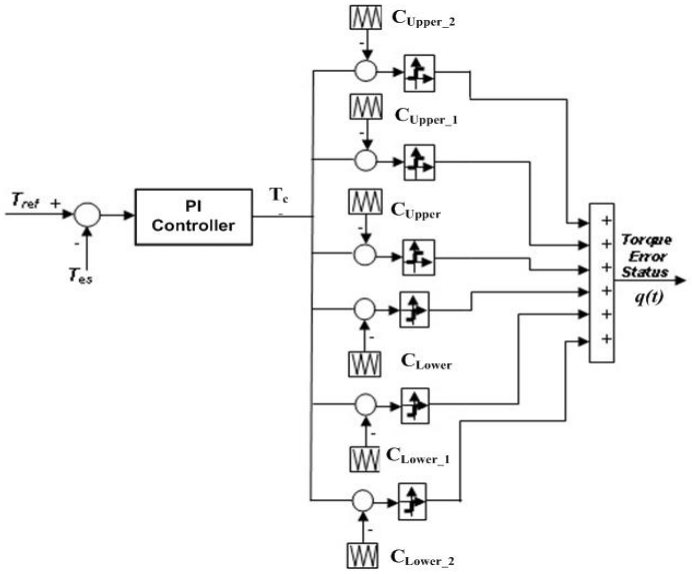

Figure 5. Proposed torque controller

The six triangular waveform generators generate 3 pairs of triangular waveforms (carrier signals) with the same magnitude but with different DC offset. Each pair (C_{Upper} and C_{Lower}) is 180° out of phase. In principle, the proposed controller will produce the same output as an 8-level hysteresis controller in [12], which can be either one of the following torque error status; 3, 2, 1, +0.5, -0.5, -1, -2, -3. The number of levels, however, must be realistic enough for implementation purposes. In other words, the higher the number of levels, the faster in terms of processor requirement is needed for implementation. By comparing the triangular waveforms with the PI controller output, a constant switching frequency can be achieved.

The instantaneous value of the torque controller output, *q(t)*, is given by (23). As for the average value of the carrier signal period, T_{tri}, designated by *d(t)* is given by (24).

$$q(t) = \begin{cases} 3, \ for & T_c \geq C_{Upper\_2} \\ 2, \ for & C_{Upper\_2} > T_c > C_{Upper\_1} \\ 1, \ for & C_{Upper\_1} > T_c > C_{Upper} \\ 0.5, \ for & C_{Upper} > T_c > 0 \\ -0.5, \ for & C_{Lower} < T_c < 0 \\ -1, \ for & C_{lower\_1} < T_c < C_{Lower} \\ -2, \ for & C_{lower\_2} < T_c < C_{Lower\_1} \\ -3, \ for & T_c \leq C_{Lower\_2} \end{cases} \tag{23}$$

$$d(t) = \frac{1}{T_{tri}} \int_t^{t+T_{tri}} q(t)dt \tag{24}$$

4.1. PI Controler's Parameter Selection

The selection of parameters value of PI controller is important to ensure the proper operation of torque controller. Hence, a linear control system theory has been used to carry out the linearizing and averaging process for the torque loop. Figure 6 shows a system torque loop.

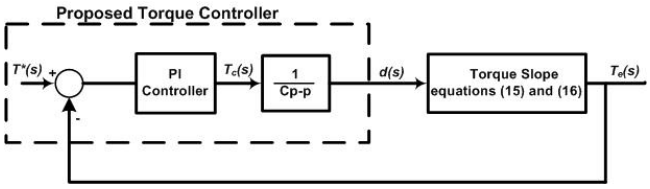

Figure 6. Torque loop

After the averaging process of (15) and (16), a simplified and averaged torque equation can be written as in (19). By introducing a small perturbation in T_e, d and ω_{slip} for linearization in (22) and transformed it to the frequency domain, the small-signal transfer function and steady state equation can be extracted as follows:

$$\widetilde{T_e}(s) = \frac{Bv_s^{\psi_s}\,\tilde{d}(s)+K\,\widetilde{\omega_{slip}}\,(s)}{s+A} \tag{25}$$

$$0 = -AT_e + B\,v_s^{\psi_s} d + K\omega_{slip} \tag{26}$$

In (25), for simplicity, $K\omega_{slip}(s)$ can be neglected since the contribution is relatively small. The complete linearized proposed torque loop is shown in Figure 7.

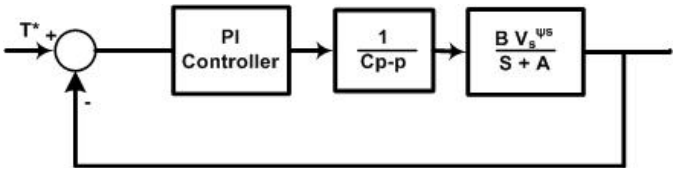

Figure 7. Linearized torque loop

Preferably, in order to obtain faster torque response, the torque loop bandwidth should be as large as it can. However, the selection of torque loop bandwidth and controller's parameters, i.e., proportional gain, K_p, and integral gain, K_i, are limited by several constraints such as hardware sampling time and carrier frequency.

The parameters of 1.5kW induction machines as listed in Table I are used to calculate the numerical values of torque loop transfer function using (19) - (20). In selecting the proportional gain of PI controller, it must be ensured that the absolute slope of control signal, T_c, is not exceed the absolute slope of the carrier signals.

Table 1. Induction Machine Parameters

Parameters	Values
Stator Resistance, R_s	3 Ω
Rotor Resistance, R_r	3.793 Ω
Stator self-inductance, L_s	0.3222 H
Rotor self-inductance, L_r	0.3308 H
Mutual inductance, L_m	0.3049 H
No. of pole, p	4
Stator flux reference, ψ_s	0.896 Wb
Voltage Vector Magnitude, $V_s^{\psi s}$	120 V

For the positive slope, as in (17), the following condition must be satisfied:

$$\langle Absolute\ slope\ of\ the\ carrier\ signal \rangle \geq \left\{-AT + BV_s^{\psi_s} + K\left(\frac{\omega_s}{d} - \omega_r\right)\right\} K_p^+ \quad (27)$$

Where the value of d in (27) is calculated from (26). For the negative slope, as in (18), the following condition must be satisfied:

$$\langle Absolute\ slope\ of\ the\ carrier\ signal \rangle \geq \{|-AT - K\ \omega_r|\} K_p^- \quad (28)$$

As the above mentioned, the torque loop bandwidth is chosen depends on the maximum bandwidth limited by the DSP sampling time or the carrier signal frequency, depending on which is lower. It is desirable to have a high carrier frequency in order to have a large torque loop bandwidth. However, the carrier signals are generated by the DSP which restricted to its sampling time. In other words, torque loop bandwidth is restricted to the software sampling time as well. To maintain the linearity between T_c and d, the carrier signals are build with eight steps per cycle. Figure 8 shows a generated carrier signal under this condition with a 75µs software sampling time. Based on the Figure 8, it shows that the carrier frequency is 1667 Hz and the absolute slope of carrier signal is 333,333.333 s^{-1}.

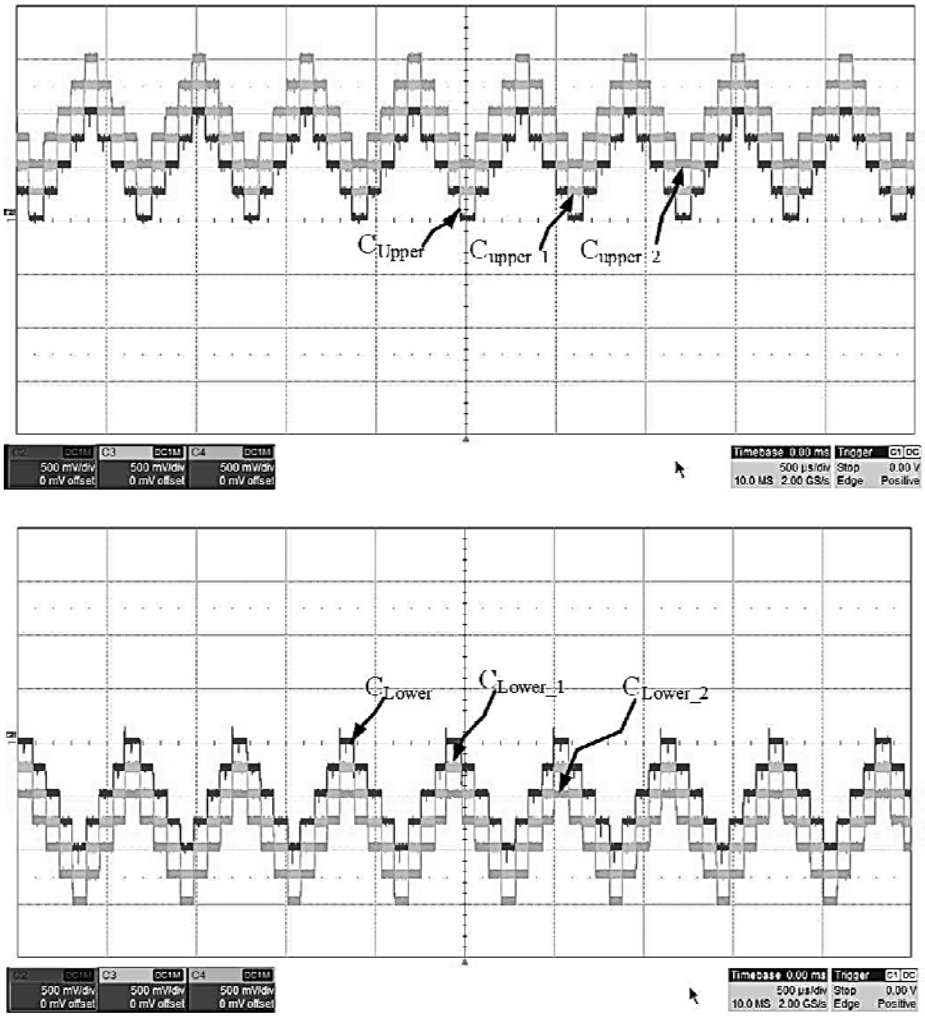

Figure 8. Generated carrier signal sampled at 75µs

The maximum proportional gain which limited by the maximum positive slopes is assumed to be occurred at zero rotor speed, ω_r=0, and at rated slip, $\omega_e = \omega_{slip}$ = 7.33 rad/s. By substituting this value and the machines parameters value into (27), gives $K_p^+ \leq 36.85$. The maximum proportional gain which is limited by

the maximum absolute negative slopes is assumed to be occurred at maximum rotor speed. As in this work, the maximum rotor speed achievable without field weakening is approximately 41 rad/s. By substituting this value and the machines parameters value into (28), gives $K_p^- \leq 90.56$. In order to ensure the control signal, T_c, is not exceeding the absolute carrier signal slope, K_p is chosen as 39.5. It should be noted that, the gain value is just an initial value that serve as a guide to operate the proposed controller. A fine tuning of the controller should be done to achieve the excellent torque response. In this work, the corresponding PI controller's parameters are chosen as K_p = 37.85 and K_i = 6169.55. The open-loop bode plot of this PI controller setting is shown in Figure 9. Based on Figure 9, the crossover frequency for this particular setting is about 3.05 kHz.

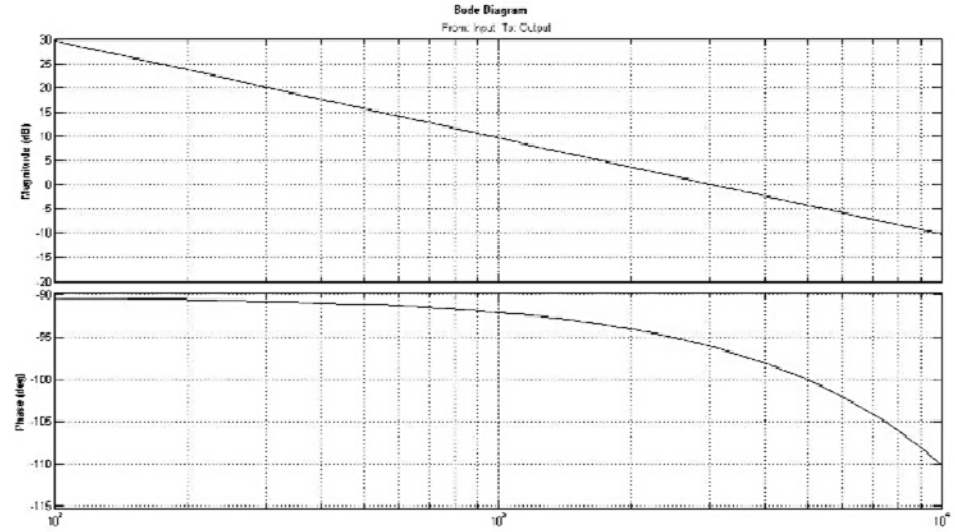

Figure 9. Bode plot of the torque loop with PI controller

5. SIMULATION AND EXPERIMENTAL RESULTS

The proposed system and a hysteresis-based system of DTC-MLI for induction machine have been simulated using MATLAB/Simulink. The parameters of PI controller that obtained in the previous section were used in the simulation as well as in the experiment. To show the feasibility of the proposed system, an experiment was also carried out. Figure 10 shows the block diagram of the experimental set-up. A dSPACE DS1104 controller card based on a TMS320F240 DSP, ALTERA DE2 FPGA board, IGBT-based 5-level CHMI, a 1.5kW squirrel-cage induction machine coupled to a DC machine was used to execute the experiment. The DS1104 was used to implement the hysteresis and the proposed controller also to estimate the torque and stator flux at a sampling period 75μs. The FPGA was used to implement the voltage vector selection table as well as to generate the blanking time for the IGBT.

The parameters of the induction machine as tabulated in Table I were used in both simulation and experiment.

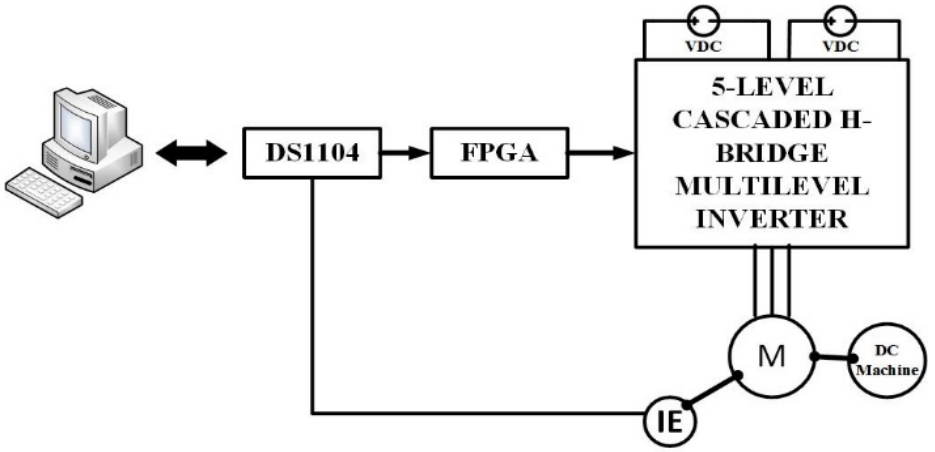

Figure 10. Experimental set-up block diagram

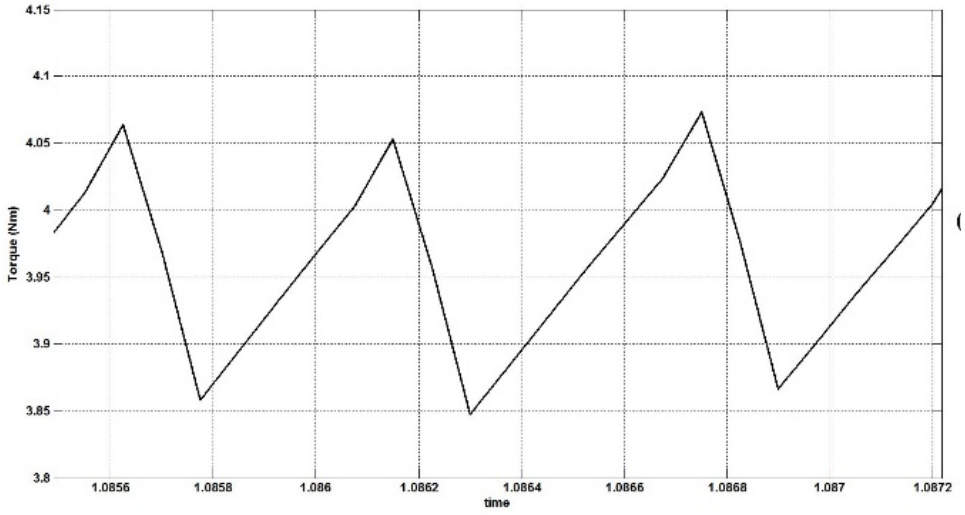

(a)

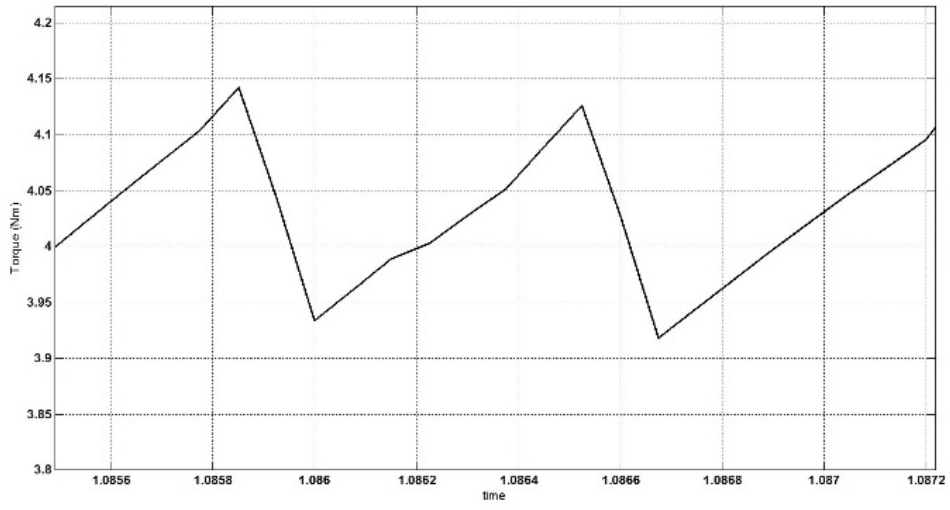

(b)

Figure 11. Simulation results of torque ripple. (a) DTC-MLI with hysteresis-based controller. (b) DTC-MLI with PI-CSF controller

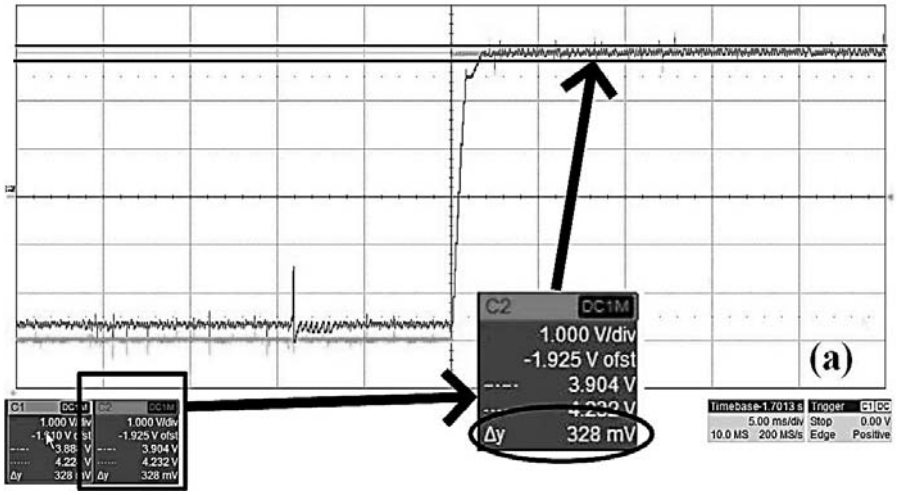

(a)

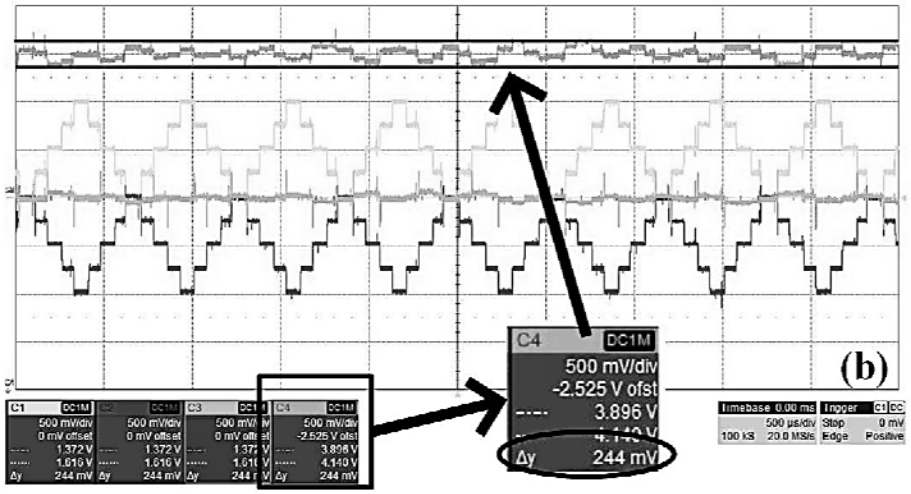

(b)

Figure 12. Experimental results of torque ripple. (a) DTC-MLI with hysteresis-based controller. (b) DTC-MLI with PI-CSF controller

Figure 11 and Figure 12 shows a simulation and experimental results of the torque ripple for DTC-MLI with hysteresis-based controller with ΔT = 0.9N.m (or 10% of the rated torque) and DTC-MLI with PI-CSF controller. Based on the experimental results, its clearly indicates that the reduction of torque ripple as much as 26% in the DTC-MLI with PI-CSF controller compared to the DTC-MLI with hysteresis-based controller. Using the PI-CSF controller, the designated controller is properly monitored and corrected the level of errors to ensure the PI controller signal is within the appropriate carrier level hence suitable voltage vector is selected either to increase or decrease the torque and been applied consecutively within a carrier waveform period. However by using the hysteresis-based controller, the voltage vector is chosen based on the comparison of the raw error signal with the hysteresis band which the selected voltage vector for increasing or decreasing the torque is applied for the entire switching period.

Figure 13 and Figure 14 show simulation and experimental results of step response for DTC-MLI with Hysteresis-based controller and DTC-MLI with PI-CSF controller respectively. Based on the experimental results, DTC-MLI with PI-CSF controller shows 5% faster performance compared to the DTC-MLI with hysteresis-based controller. In DTC-MLI with PI-CSF controller, the designated controller first filtered and processed the torque error to ensure the large error will appropriately trigger the correct carrier signal. As a result, the voltage vector with the highest torque increment (or decrement) is selected for large errors hence produce faster torque response. In contrast, the raw torque error signal in the DTC-MLI with hysteresis-based controller is directly controlled by the hysteresis bands which produce a slower response.

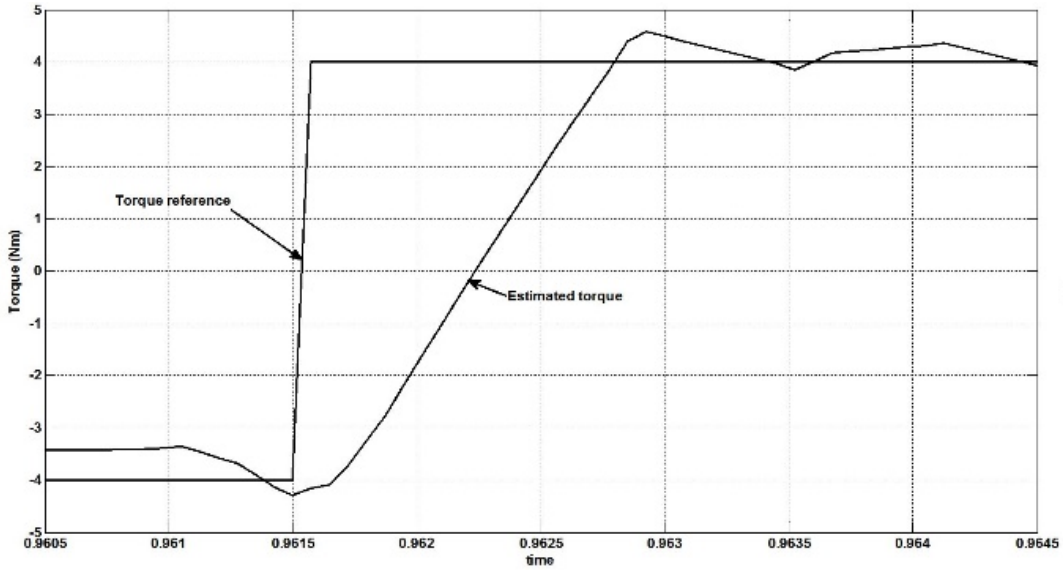

(a)

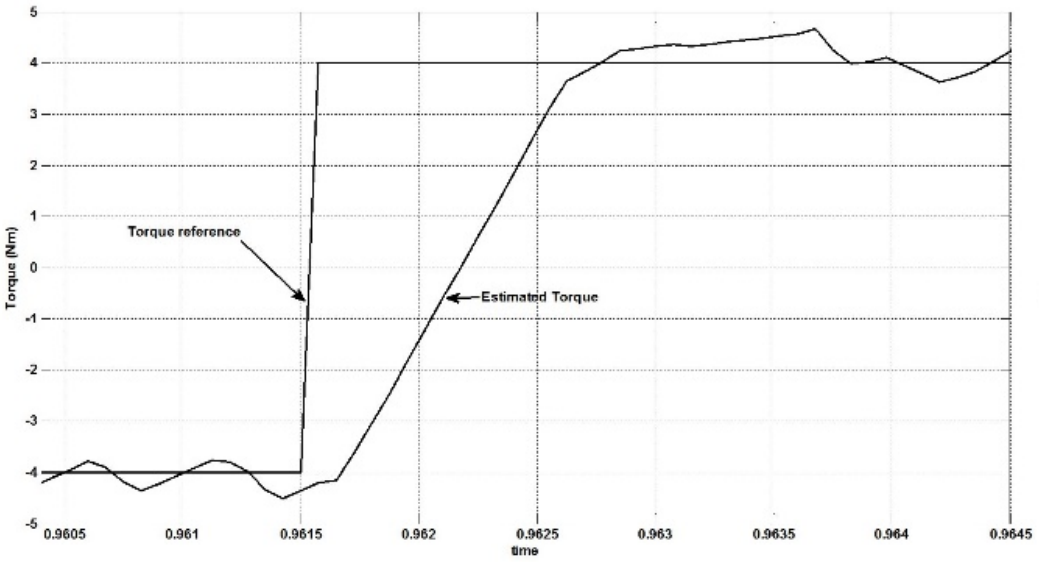

(b)

Figure 13. Simulation results of torque response. (a) DTC-MLI with hysteresis-based controller. (b) DTC-MLI with PI-CSF controller

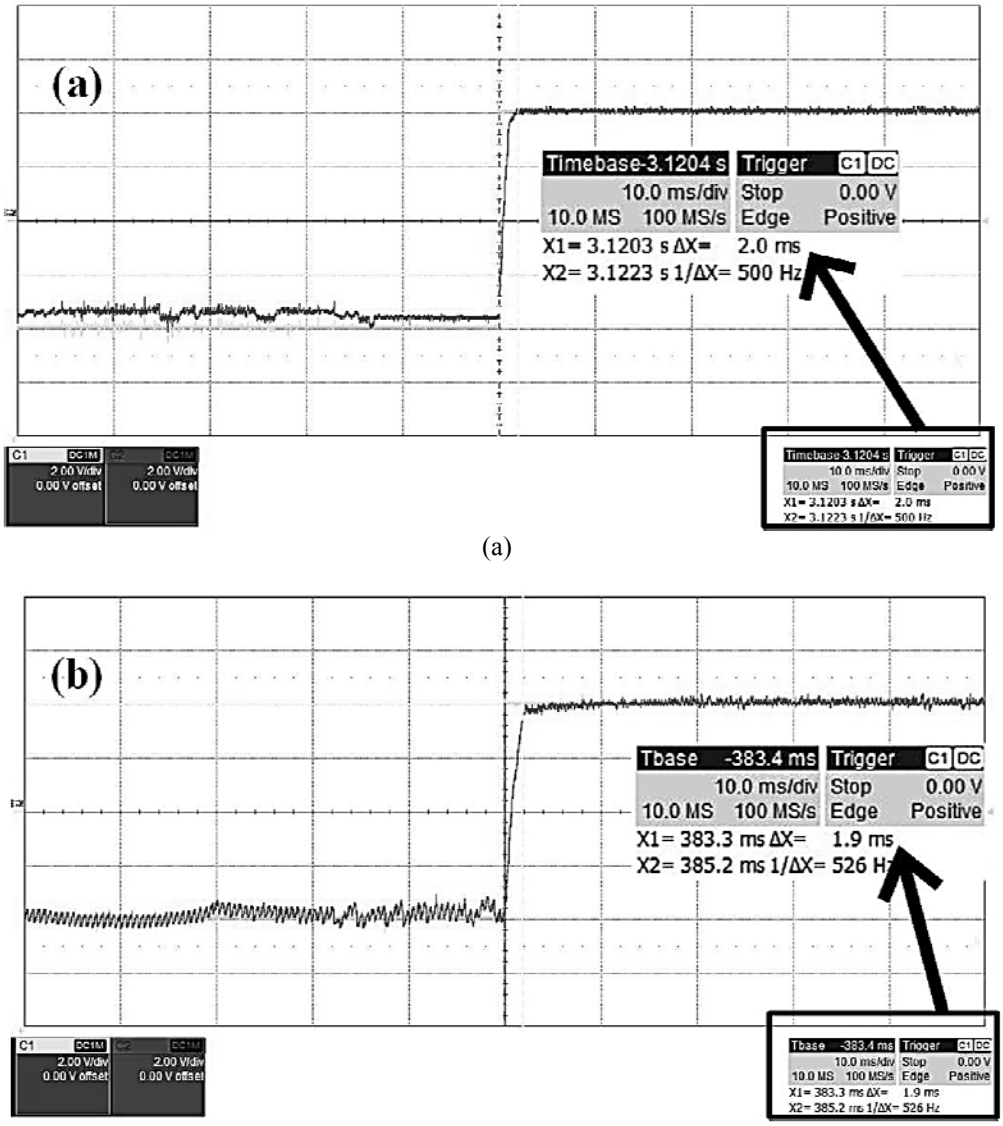

(a)

(b)

Figure 14. Experimental results of torque response. (a) DTC-MLI with hysteresis-based controller. (b) DTC-MLI with PI-CSF controller

The frequency spectrum of the phase voltage for both simulation and experimental results of the DTC-MLI with Hysteresis-based controller and DTC-MLI with PI-CSF controller are shown in Figure 15 and Figure 16 respectively. For the DTC-MLI with PI-CSF controller, the dominant harmonics is at the carrier frequency of about 1667 Hz. On the contrary, a widely distributed harmonics in the frequency spectrum with an unpredictable switching frequency is obtained for DTC-MLI with hysteresis-based controller. The unpredictable switching frequency is undesirable since the switching capability of the inverter is not fully utilized. In addition, it will create an unpredictable harmonics in current flow. Figure 17 shows a simulation results for multilevel inverter line-to-line voltage (V_{AB}).

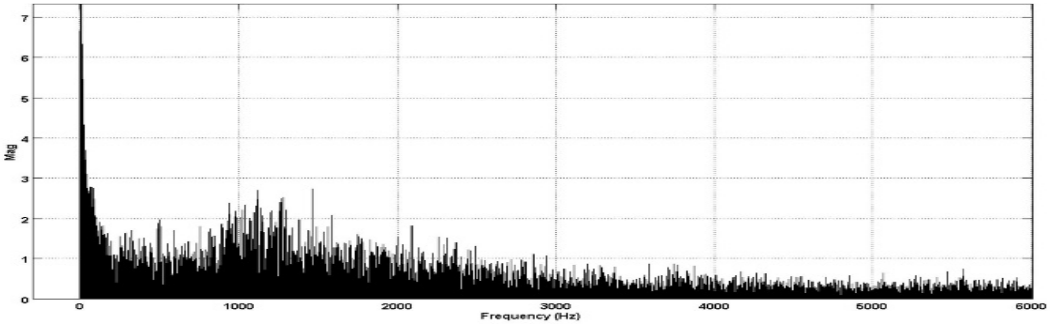

(a)

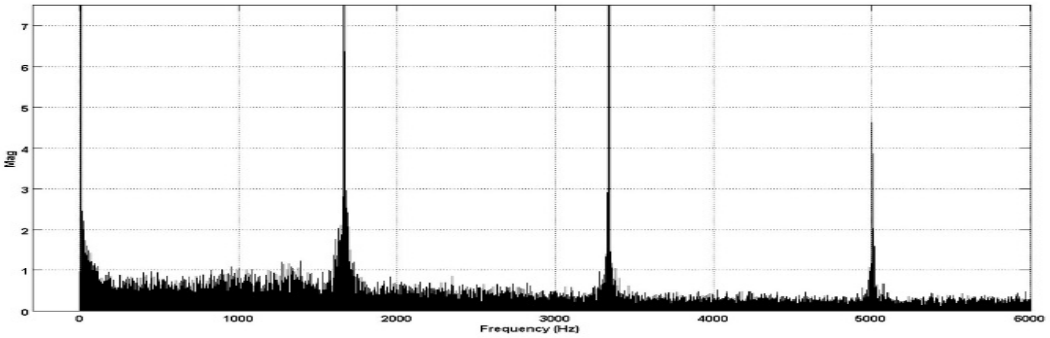

(b)

Figure 15. Simulation results of the frequency spectrum of phase voltage. (a) DTC-MLI with hysteresis-based controller. (b) DTC-MLI with PI-CSF controller

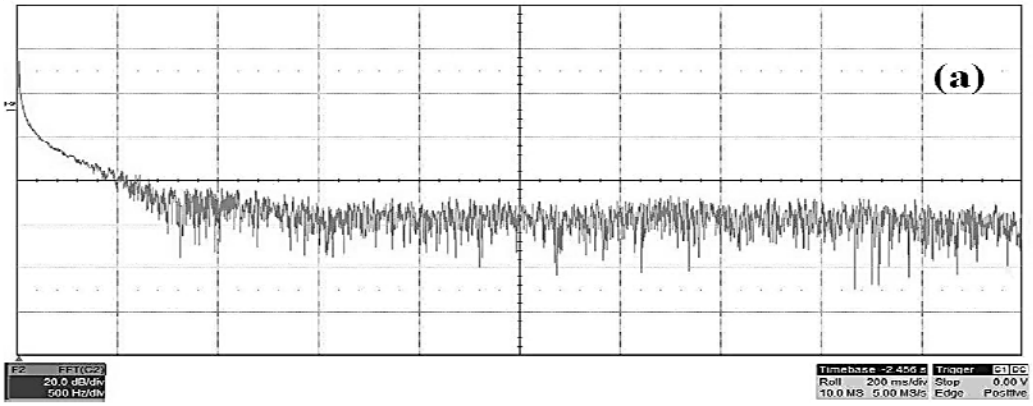

(a)

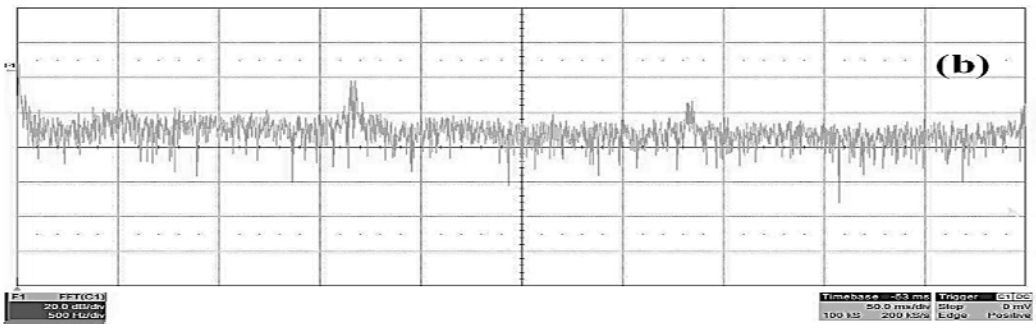

(b)

Figure 16. Experimental results of the frequency spectrum of phase voltage. (a) DTC-MLI with hysteresis-based controller. (b) DTC-MLI with PI-CSF controller

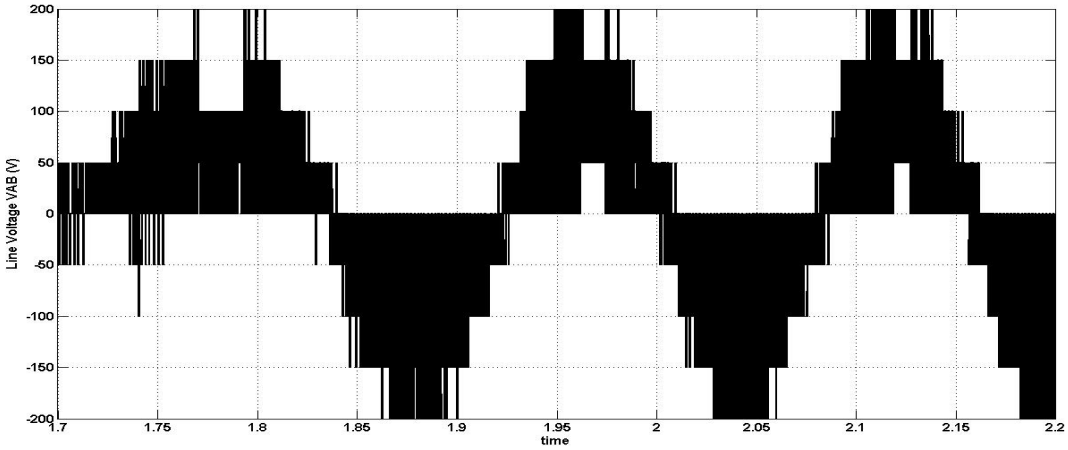

(a)

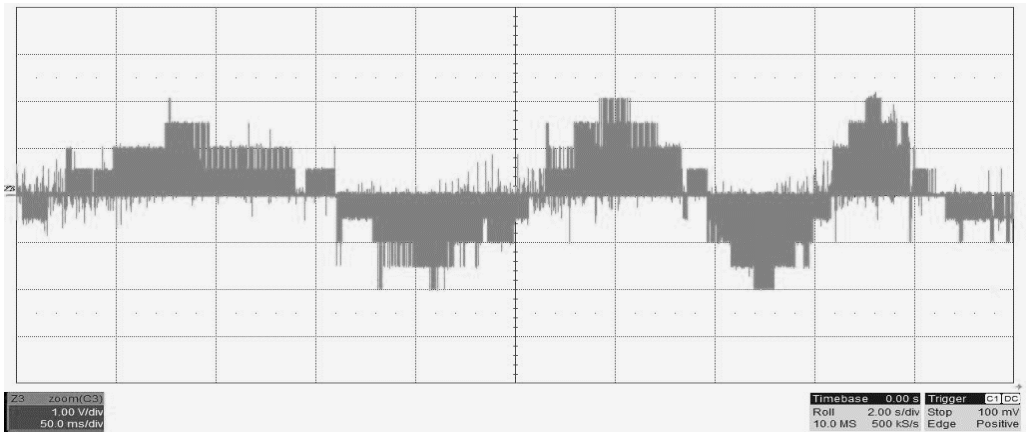

(b)

Figure 17. Line-to-line voltage (V_{AB}) for 5-level cascaded H-bridge multilevel inverter. (a) Simulation. (b) Experiment ; scale : 1V/div = 100V

6. CONCLUSION

A PI-CSF torque controller to enhance the DTC-MLI system has been proposed. With the proposed controller, torque ripples are reduced and the switching frequency can be retained at a fixed value. The operational concept together with the derivation of the proposed controller linear model has been presented. The feasibility of the proposed controller is demonstrated by hardware implementation. A dSPACE DS1104 controller card based on a TMS320F240 DSP together with ALTERA DE2 FPGA board were used to execute the experiment. From the results, this simple scheme has significantly improved the performance of the DTC-MLI drive system yet maintained the simple structure of the DTC drive.

ACKNOWLEDGMENT

The author would like to thanks the Ministry of Higher Education of Malaysia for the financial funding of this project with vote number R.J130000.7823.3F523 and R.J130000.7808.4F799, also the Research Management Center (RMC) of Universiti Teknologi Malaysia for their support on research management and funding with vote number Q.J130000.2525.05H87 and Q.J130000.2523.05H26.

REFERENCES

[1] I. Takahashi and T. Noguchi, "A new quick-response and high-efficiency control strategy of an induction motor", *IEEE Transactions on Industry Applications,* pp. 820-827, 1986.
[2] U.V. Patil, H.M. Suryawanshi, and M.M. Renge, "Closed-loop hybrid direct torque control for medium voltage induction motor drive for performance improvement", *IET Power Electronics,* vol. 7, pp. 31-40, 2014.

[3] N.M. Nordin, N.R.N. Idris, N.A. Azli, and M.Z. Puteh, "Fuzzy-PI Torque and Flux Controllers for DTC with Multilevel Inverter of Induction Machines", *International Journal of Power Electronics and Drive Systems (IJPEDS),* vol. 5, pp. 268-282, 2014.
[4] D. Islam, C. Reza, and S. Mekhilef, "DTC-IM drive with 5-level hybrid cascaded h-bridge inverter", in *Industrial Electronics and Applications (ICIEA), 2014 IEEE 9th Conference on*, 2014, pp. 332-337.
[5] P. Alagappan and R. Dhanasekaran, "Implementation of Fuzzy Logic Based Direct Torque Control of Induction Motor", *International Journal of Electrical and Electronics Engineering Advance Research,* vol. 2, pp. 183-187, 2014.
[6] S.P. Yalla, P. Pugazhendiran, and K. Beagam, "Synthesized Direct Torque Control for high-power induction motor drive", in *Intelligent Systems and Control (ISCO), 2013 7th International Conference on*, 2013, pp. 79-83.
[7] A. Alqudah, M. Mohaidat, and I. Altawil, "Control of variable speed drive (VSD) based on diode clamped multilevel inverter using direct torque control and fuzzy logic", in *Applied Electrical Engineering and Computing Technologies (AEECT), 2013 IEEE Jordan Conference on*, 2013, pp. 1-6.
[8] N.F. Alias, A. Jidin, M.A. Said, A.R. Abdullah, H. Jopri, and N.H. Rahim, "Improved performance of Direct Torque Control of Induction Machine with 3-level Neutral Point Clamped multilevel inverter", in *Electrical Machines and Systems (ICEMS), 2013 International Conference on*, 2013, pp. 2110-2114.
[9] Y. Zhang, J. Zhu, Z. Zhao, W. Xu, and D.G. Dorrell, "An improved direct torque control for three-level inverter-fed induction motor sensorless drive", *Power Electronics, IEEE Transactions on,* vol. 27, pp. 1502-1513, 2012.
[10] U. Patil, H. Suryawanshi, and M. Renge, "Torque Ripple Minimization in Direct Torque Control Induction Motor Drive Using Space Vector Controlled Diode-clamped Multi-level Inverter", *Electric Power Components and Systems,* vol. 40, pp. 792-806, 2012.
[11] T. Geyer and S. Mastellone, "Model predictive direct torque control of a five-level ANPC converter drive system", *Industry Applications, IEEE Transactions on,* vol. 48, pp. 1565-1575, 2012.
[12] N.M. Nordin, N.R.N. Idris, and N.A. Azli, "Direct Torque Control with 5-level cascaded H-bridge multilevel inverter for induction machines", in *IECON 2011 - 37th Annual Conference on IEEE Industrial Electronics Society*, Melbourne, VIC Australia, 2011, pp. 4691-4697.
[13] A. Mortezaei, N.A. Azli, N.R.N. Idris, S. Mahmoodi, and N.M. Nordin, "Direct torque control of induction machines utilizing 3-level cascaded H-Bridge Multilevel Inverter and fuzzy logic", in *Applied Power Electronics Colloquium (IAPEC), 2011 IEEE* Johor Bahru, Malaysia, 2011, pp. 116-121.
[14] F. Khoucha, M.S. Lagoun, A. Kheloui, and M. El Hachemi Benbouzid, "A comparison of symmetrical and asymmetrical three-phase H-bridge multilevel inverter for DTC induction motor drives", *Energy Conversion, IEEE Transactions on,* vol. 26, pp. 64-72, 2011.
[15] Y. Zhang, J. Zhu, Z. Zhao, W. Xu, and D.G. Dorrell, "An Improved Direct Torque Control for Three-Level Inverter-Fed Induction Motor Sensorless Drive", *Power Electronics, IEEE Transactions on,* p. 1, 2010.
[16] L. Youb, A. Craciunescu, and G. Ciumbulea, "A new fuzzy logic direct torque control scheme of induction motor for electrical vehicles application", in *XIX International Conference on Electrical Machines (ICEM), 2010* Rome, 2010, pp. 1-6.
[17] P. Urrejola, M. Perez, J. Rodriguez, and M. Trincado, "Direct torque control of an 3L-NPC inverter-fed induction machine: A model predictive approach", in *IECON 2010 - 36th Annual Conference on IEEE Industrial Electronics Society* Glendale, AZ, 2010, pp. 2947-2952.
[18] T.R. Obermann, Z.D. Hurst, and R.D. Lorenz, "Deadbeat-direct torque & flux control motor drive over a wide speed, torque and flux operating space using a single control law", in *Energy Conversion Congress and Exposition (ECCE), 2010 IEEE* Atlanta, GA 2010, pp. 215-222.
[19] S.X. Liu, M.Y. Wang, Y.G. Chen, and S. Li, "A novel fuzzy direct torque control system for three-level inverter-fed induction machine", *International Journal of Automation and Computing,* vol. 7, pp. 78-85, 2010.
[20] F. Khoucha, S.M. Lagoun, K. Marouani, A. Kheloui, and M. El Hachemi Benbouzid, "Hybrid cascaded H-bridge multilevel-inverter induction-motor-drive direct torque control for automotive applications", *Industrial Electronics, IEEE Transactions on,* vol. 57, pp. 892-899, 2010.
[21] H. Alloui, A. Berkani, and H. Rezine, "A three level NPC inverter with neutral point voltage balancing for induction motors Direct Torque Control", in *XIX International Conference on Electrical Machines (ICEM), 2010*, Rome, 2010, pp. 1-6.
[22] J. Pereda, J. Dixon, and M. Rotella, "Direct Torque Control for sensorless induction motor drives using an improved H-Bridge multilevel inverter", in *Industrial Electronics, 2009. IECON '09. 35th Annual Conference of IEEE* Alfandega Congress Center Porto, Portugal, 2009, pp. 1110-1115.
[23] F. Khoucha, S.M. Lagoun, K. Marouani, A. Kheloui, and M.E.H. Benbouzid, "Hybrid cascaded H-bridge multilevel inverter motor drive DTC control for Electric Vehicles", 2009, pp. 1-6.
[24] R. Zaimeddine, L. Refoufi, and E.M. Berkouk, "An Improved Direct Torque Control Strategy for Induction Motor Drive", *International Journal of Electrical and Power Engineering, Medwell Journals,* vol. 1, pp. 21 - 27, 2007.
[25] R. Toufouti, S. Meziane, and H. Benalla, "Direct Torque Control for Induction Motor Using Intelligent Techniques", *Journal of Theoretical and Applied Information Technology,* 2007.
[26] S. Kouro, R. Bernal, H. Miranda, C.A. Silva, and J. Rodriguez, "High-performance torque and flux control for multilevel inverter fed induction motors", *IEEE Transactions on Power Electronics,* vol. 22, pp. 2116-2123, 2007.
[27] P. Correa, M. Pacas, and J. Rodriguez, "Predictive torque control for inverter-fed induction machines", *IEEE Transactions on Industrial Electronics,* vol. 54, pp. 1073-1079, 2007.
[28] Y. Wang, H. Li, and X. Shi, "Direct Torque Control with Space Vector Modulation for Induction Motors Fed by Cascaded Multilevel Inverters", 2006, pp. 1575-1579.

[29] S. Kouro, R. Bernal, H. Miranda, J. Rodriguez, and J. Pontt, "Direct Torque Control With Reduced Switching Losses for Asymmetric Multilevel Inverter Fed Induction Motor Drives", 2006.
[30] J. Rodríguez, J. Pontt, S. Kouro, and P. Correa, "Direct torque control with imposed switching frequency in an 11-level cascaded inverter", *IEEE Transactions on Industrial Electronics,* vol. 51, pp. 827-833, 2004.
[31] X. del Toro, S. Calls, M.G. Jayne, P.A. Witting, A. Arias, and J.L. Romeral, "Direct torque control of an induction motor using a three-level inverter and fuzzy logic", in *Industrial Electronics, 2004 IEEE International Symposium on*, 2004, pp. 923-927 vol. 2.
[32] M.F. Escalante, J.C. Vannier, and A. Arzande, "Flying capacitor multilevel inverters and DTC motor drive applications", *IEEE Transactions on Industrial Electronics,* vol. 49, pp. 809-815, 2002.
[33] S. Krim, S. Gdaim, A. Mtibaa, and M.F. Mimouni, "Real Time Implementation of High Performance's Direct Torque Control of Induction Motor on FPGA", *International Review of Electrical Engineering (IREE),* vol. 9, pp. 919-929, 2014.
[34] T. Ramesh, A.K. Panda, S.S. Kumar, and S. Bonala, "High performance direct torque and flux control of induction motor drive using fuzzy logic based speed controller", in *Circuits, Power and Computing Technologies (ICCPCT), 2013 International Conference on*, 2013, pp. 213-218.
[35] S. Krim, S. Gdaim, A. Mtibaa, and M.F. Mimouni, "FPGA-Based Implementation Direct Torque Control of Induction Motor", *International Journal of Power Electronics and Drive Systems (IJPEDS),* vol. 5, pp. 293-304, 2015.
[36] R. Gunabalan and V. Subbiah, "Speed Sensorless Vector Control of Induction Motor Drive with PI and Fuzzy Controller", *International Journal of Power Electronics and Drive Systems (IJPEDS),* vol. 5, pp. 315-325, 2015.
[37] N.R.N. Idris, C.L. Toh, and M.E. Elbuluk, "A new torque and flux controller for direct torque control of induction machines", *IEEE Transactions on Industry Applications,* vol. 42, pp. 1358-1366, 2006.
[38] N.R.N. Idris and A.H.M. Yatim, "Direct torque control of induction machines with constant switching frequency and reduced torque ripple", *IEEE Transactions on Industrial Electronics,* vol. 51, pp. 758-767, 2004.
[39] J.K. Kang and S.K. Sul, "Analysis and prediction of inverter switching frequency in direct torque control of induction machine based on hysteresis bands and machine parameters", *Industrial Electronics, IEEE Transactions on,* vol. 48, pp. 545-553, 2001.
[40] D. Casadei, G. Serra, and A. Tani, "Analytical investigation of torque and flux ripple in DTC schemes for induction motors", in *Industrial Electronics, Control and Instrumentation, 1997. IECON 97. 23rd International Conference on*, 1997, pp. 552-556.

BIOGRAPHIES OF AUTHORS

Norjulia Mohamad Nordin received her Bachelor's degree in Electrical Engineering from Universiti Teknologi Malaysia, Johor, Malaysia, in 2006 and the M. Eng. Sc. Degree in Energy System from The University of New South Wales, Australia, in 2008. She is currently working towards her Ph.D. degree in the Universiti Teknologi Malaysia, Johor, Malaysia. Her current research interests are AC drive system with multilevel inverter and field programmable gate array application for drive system.

Naziha Ahmad Azli received her B. Sc. Degree in Electrical Engineering from University of Miami, Florida, USA and M.E.E. and Ph.D. from Universiti Teknologi Malaysia in 1986, 1992 and 2002 respectively. She is now an Associate Professor at Universiti Teknologi Malaysia (UTM) with which she has been affiliated since 1988. She currently teaches Power Electronics at both undergraduate and post-graduate levels at the university. Her research interests are power quality, renewable / alternate / distributed energy and intelligent systems applied to power electronics converters.

Nik Rumzi Nik Idris (M'97–SM'03) received the B.Eng. degree in electrical engineering from the University of Wollongong, Wollongong, Australia, in 1989, the M.Sc. degree in power electronics from Bradford University, Bradford, U.K., in 1993, and the Ph.D. degree from the Universiti Teknologi Malaysia, Johor, Malaysia, in 2000. He was a Visiting Research Associate at the University of Akron, Akron, OH, in 2002. Currently, he is an Associate Professor at the Universiti Teknologi Malaysia. His research interests include AC drive systems and DSP applications in power electronic systems. He is a Senior Member of the IEEE Industry Applications, IEEE Industrial Electronics, and IEEE Power Electronics Societies.

Nur Huda Ramlan received her Bachelor's degree in Electrical and Electronics Engineering from Universiti Teknologi Petronas, Perak, Malaysia, in 2009 and the M. Eng. in Electrical from University Teknologi Malaysia, Johor, Malaysia in 2011. She is currently working towards her Ph.D. degree in the Universiti Teknologi Malaysia. Her current research interests are passivity based controller, active power filters and multilevel inverters.

Tole Sutikno is an Associated Professor in Department of Electrical Engineering at Universitas Ahmad Dahlan (UAD), Indonesia. He is Editor-in-Chief, Principle Contact and Editor for some Scopus indexed journals. He is also one of founder of the Indonesian Publication Index (IPI). He has completed his studies for B.Eng., M.Eng., Ph.D. in Electrical Engineering from Diponegoro University, Gadjah Mada University and Universiti Teknologi Malaysia, respectively. His research interests include the field of industrial electronics and informatics, power electronics, FPGA applications, embedded systems, data mining, information technology and digital library.